DOI: 10.19113/sdufenbed.1674189

Annealing Effects on Cu₂ZnSnSe₄ Thin Films: Structural, Electrical, and Optical Characterization

Duygu TAKANOGLU BULUT*10, Koray YILMAZ20, Orhan KARABULUT30

¹Pamukkale Üniversitesi, İleri Teknoloji Uygulama ve Araştırma Merkezi, 20160, Denizli, Türkiye

^{2,3}Pamukkale Üniversitesi, Fen Fakültesi, Fizik Bölümü, 20160, Denizli, Türkiye

(Alınış / Received: 11.04.2025, Kabul / Accepted: 01.07.2025, Online Yayınlanma / Published Online: 25.08.2025)

Keywords

Cu₂ZnSnSe₄ Thin Film, Thermal Evaporation, Structural Characterization, Hall Effect **Abstract:** This study aims to explore the effects of annealing on the structural, electrical, and optical properties of $\mathrm{Cu_2ZnSnSe_4}$ thin films deposited by thermal evaporation. Results obtained from SEM equipped with EDAX, XRD, and Raman analysis revealed that CZTSe thin films were successfully obtained. Depending on the annealing temperature, increasing grain size and shifting from spherically shaped grains to rod-shaped particles were observed. The room temperature resistivity decreased with increasing annealing temperature, exhibiting values of 44.10, 2.61, and 3.08 Ω -cm for films annealed at 400 °C, 500 °C, and 600 °C, respectively. Carrier concentrations of the same samples obtained from Hall Effect measurements were observed as 5.13×10^{15} , 3.07×10^{17} , and 1.09×10^{17} cm⁻³ with p-type conductivity. The as-deposited and annealed thin films exhibited optical band gap values of 1.98, 1.78, 1.35, and 1.65 eV, respectively.

Cu₂ZnSnSe₄ İnce Filmleri Üzerindeki Tavlama Etkileri: Yapısal, Elektriksel ve Optik Karakterizasyon

Anahtar Kelimeler Cu₂ZnSnSe₄ İnce Film, Termal Buharlaştırma, Yapısal Karakterizasyon,

Hall Etkisi

Öz: Bu çalışma, termal buharlaştırma yöntemiyle üretilen $Cu_2ZnSnSe_4$ ince filmlerin yapısal, elektriksel ve optik özellikleri üzerine tavlama işleminin etkilerini araştırmayı amaçlamaktadır. SEM-EDAX, XRD ve Raman analizlerinden elde edilen sonuçlar, CZTSe ince filmlerin başarılı bir şekilde üretildiğini ortaya koymuştur. Tavlama sıcaklığına bağlı olarak, tane boyutunda artış ve küresel şekilli tanelerden çubuk biçimli yapılara doğru bir morfolojik dönüşüm gözlemlenmiştir. Oda sıcaklığındaki özdirencin, artan tavlama sıcaklığı ile birlikte azaldığı belirlenmiş; bu değerler sırasıyla 400 °C, 500 °C ve 600 °C'de tavlanan filmler için 44,10, 2,61 ve 3,08 Ω -cm olarak ölçülmüştür. Aynı örnekler için Hall etkisi ölçümleriyle elde edilen taşıyıcı yoğunlukları sırasıyla 5,13×10¹⁵, 3,07×10¹⁷ ve 1,09×10¹⁷ cm⁻³ olup, tüm örneklerde p-tipi iletkenlik gözlemlenmiştir. Tavlanmamış ve tavlanmış ince filmler sırasıyla 1,98, 1,78, 1,35 ve 1,65 eV optik bant aralığı değerleri sergilemiştir.

1. Introduction

Thin-film solar cells using chalcopyrite semiconductor materials have become an important research topic in recent years. Solar cells based on CuInGaSe₂ (CIGS) and CuInGa(Se,S)₂ have exhibited efficiencies of around 20% and 23%, respectively, as reported in the literature [1-5]. However, recently, one of the main problems faced by CIGS-based solar cells, the price of indium and gallium elements, has been constantly increasing due to a higher global demand than supply.

In addition, indium and gallium are widely used in areas such as producing flat-screen LCD TVs and optoelectronic fields [6,,7]. For this reason, researchers are focused on producing solar cells with similar properties but without using indium and gallium.

In recent years, researchers have begun to use the $Cu_2ZnSnSe_4$ compound as an absorber layer for thin film solar cells. $Cu_2ZnSnSe_4$ offers a sustainable alternative to CIGS, as it is composed of non-toxic and

earth-abundant elements such as Cu, Zn, Sn, and Se. For this reason, Friedlmeier et al. have suggested that the Cu₂ZnSnSe₄ compound is a promising candidate for the absorber layer that belongs to the I₂-II-IV-VI₄ semiconductor family [8,9]. Hereafter, Cu₂ZnSn(S,Se)₄ derived thin film solar cells using different deposition methods were reported, and efficiencies were found to be around 10% [10-14].

In 2013, the IBM group reported the efficiency of solar cells comprising $Cu_2ZnSn(S,Se)_4$ 11.1%, which was deposited by hydrazine-based liquid coating [15.,16]. Subsequently, in 2014, $Cu_2ZnSn(S,Se)_4$ -based solar cells, fabricated via a toxic hydrazine (N_2H_4) solution process, achieved a maximum efficiency of 12.6% [10.,17]. More recently, further advancements have been made; in 2023, an efficiency of 13.6% was reported through controlled selenization processes [18], and in 2024, a record efficiency of 15.4% (certified 14.9%) was achieved by employing a vacancy-assisted cation rearrangement strategy [19].

The physical properties of these films have been investigated by many researchers, and different synthesis methods have been reported. It is reported that $Cu_2ZnSnSe_4$ has a high absorption coefficient (> 10^4 - 10^5 cm^{-1}) and direct band gap (~0.9-1.54 eV), which closely matches the solar spectrum [9.,20-22]. It also shows p-type conductivity and has a carrier concentration of films ranging from 10^{17} - 10^{19} cm^{-3} [23-26]. Additionally, $Cu_2ZnSnSe_4$ is also an earthabundant and low-cost raw material, which is required for low-cost photovoltaics [7]. These properties indicate that $Cu_2ZnSnSe_4$ thin films can be considered strong candidates for absorber layers in solar cells.

Regardless of the deposition techniques, the film's characterization with respect to temperature dependent electrical and optical properties is an open subject in the literature. This study aimed to fabricate Cu₂ZnSnSe₄ thin films by employing the thermal evaporation technique with a single crucible. Subsequently, detailed temperature-dependent electrical characterization was carried out between 10 and 400 K using Hall effect measurements to determine the fundamental requirements for photovoltaic applications. The as-deposited films were annealed at various temperatures, and the annealing effects on the structural, optical, and electrical properties of the thin films were systematically characterized.

2. Materials and Methods

 ${\rm Cu_2ZnSnSe_4}$ (CZTSe) thin films, approximately 0.5 μm in thickness, were prepared onto soda-lime glass substrates pre-treated by chemical and ultrasonic cleaning, using a Vaksis-PVD-Handy thermal evaporation system. Stoichiometric amounts of copper, zinc, tin, and selenium, each with 4Ns purity,

were employed to prepare the precursor material for evaporation. Source elements were placed into a cleaned quartz crucible, which was subsequently sealed under vacuum. To ensure complete synthesis and compositional uniformity, the crucible was slowly heated up to 1200 $^{\circ}C$ while the tubes were continuously shaken. The crucible was subjected to heat treatment for 48 h at this temperature, and after synthesis, the furnace was slowly cooled to ambient temperature. The precursor material for evaporation was subsequently obtained by grinding the resulting ingot into a fine powder. The evaporation source was placed into a tungsten boat, and thin films were subsequently deposited via the thermal evaporation technique. Film thickness and evaporation rate were precisely controlled by employing a thickness monitor. During evaporation, the pressure was kept constant at 10^{-5} Torr, and the thin film deposition was performed at a rate of 20 Å/s.

The 'as-deposited' samples were annealed in an N_2 environment at 400 °C, 500 °C, and 600 °C for one hour, and the effect of annealing of $Cu_2ZnSnSe_4$ thin films on structural, optical, and electrical characteristics was examined.

X-ray diffraction analysis (Rigaku SmartLab, Japan) using $CuK\alpha$ radiation was employed to characterize the crystalline structure of the thin films. Field emission scanning electron microscopy (FESEM, JEOL JSM-7600F, Japan) was employed to examine the microstructure of the films. Raman spectra of the samples were obtained using a Raman spectrometer (BWTEK BWS465-785S, USA) integrated with a CCD detector, in a backscattering geometry, and employing a 785 nm laser as the excitation source. Temperaturedependent Hall effect measurements were performed using a Keithley 2400 source-measure unit and a Keithley 2700 electrometer assembled with a Keithley 7709 matrix card. For Hall measurements, a magnetic field of 1.2 T, generated by a GMW magnet, was applied perpendicular to the film layers. The temperature was precisely controlled and monitored using a LakeShore 331 temperature controller. Optical absorption properties were investigated using a UNICO SQ 2802 UV/VIS spectrophotometer.

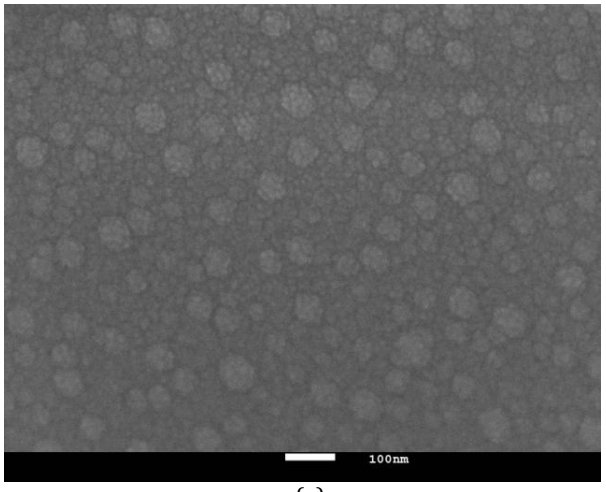
3. Results and Discussions

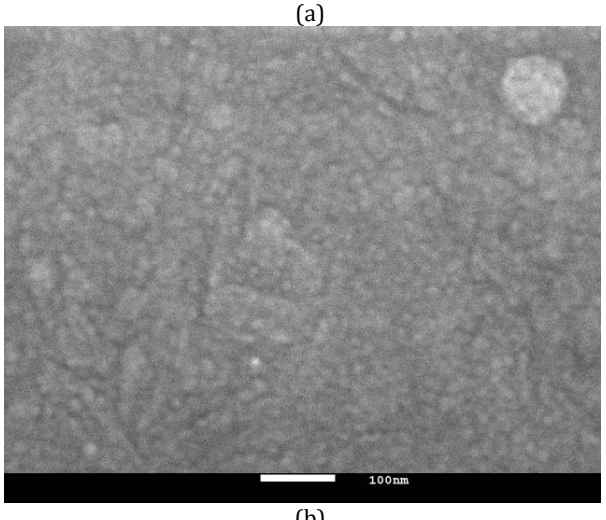
Thermally evaporated thin films were labeled according to their annealing conditions, as shown in Table 1.

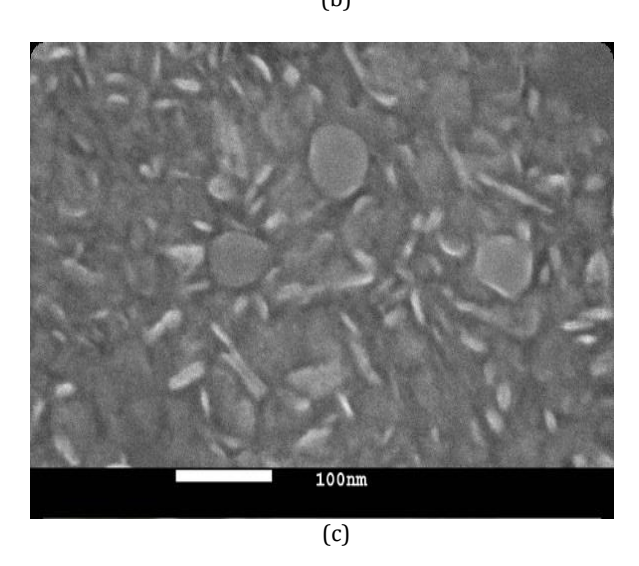
Table 1. Labels of the thin films according to the temperature of annealing

Sample	Annealing Temperature (°C)			
T0	-			
T400	400			
T500	500			
T600	600			

FESEM was employed to examine the microstructure of the thin films, as it provides detailed information on surface morphology. The corresponding surface images are presented in Figure 1.







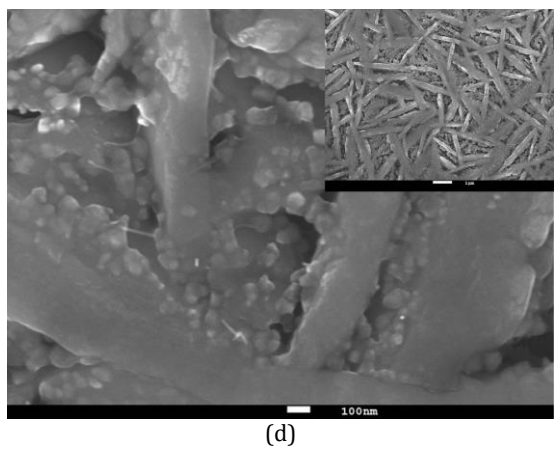


Figure 1. FESEM images of thin films (a) T0, (b) T400, (c) T500, (d) T600 (The inset shows a higher magnification image of the T600 film with a 1 μ m scale bar)

From the comparison of the micrographs, it was determined that the crystallization of the films was enhanced with annealing temperature, and the grain morphology was transformed from spherical to rodshaped particles. It is observed that all films are homogeneous and covered with uniform grains, and the size of grains increases with annealing temperature. J. Iljina et al. reported that increasing the selenization duration led to larger crystal sizes, with crystals of 1.5–4 μm observed in films annealed for 60 minutes at 470 °C [27]. In a subsequent study on Cu₂ZnSnSe₄, S. Hong et al. annealed thin films at various temperatures ranging from 350 $^{\circ}C$ to 650 $^{\circ}C$. It was reported that annealing at 550, 600, and 650 $^{\circ}C$ caused an increase in grain size [28]. In a different study, D. H. Kuo et al. fabricated Cu₂ZnSnSe₄ thin films via sputtering Cu-Zn-Sn metallic precursors and selenization at 500-600 °C. After selenization at higher temperatures, a suitable microstructure with large and uniform grains was reported for Cu₂ZnSnSe₄ films [25]. Consistent with these findings, previous studies have also shown that elevated selenization and substrate temperatures lead to increased grain size [11.,29-31].

The stoichiometry of both the source material and the thin films was conducted with an FESEM coupled with an EDAX detector. The atomic weight percentages of Cu, Zn, Sn, and Se in the powder compound were measured as 21.02%, 15.32%, 16.52%, and 47.15%, respectively. The EDAX spectrum revealed no impurities in the source material, and the stoichiometry was found to be nearly consistent with the ideal 2:1:1:4 ratio. In Figure 2, the EDAX spectra corresponding to both the synthesized source material and the thin films annealed at various temperatures are presented. The obtained spectra confirm the presence of Cu, Zn, Sn, and Se in both the as-deposited and annealed films, indicating that the annealing process did not induce any alteration in the fundamental chemical composition of the films. This observation suggests that, despite the structural reorganization induced by thermal treatment, the chemical integrity of the films was preserved.

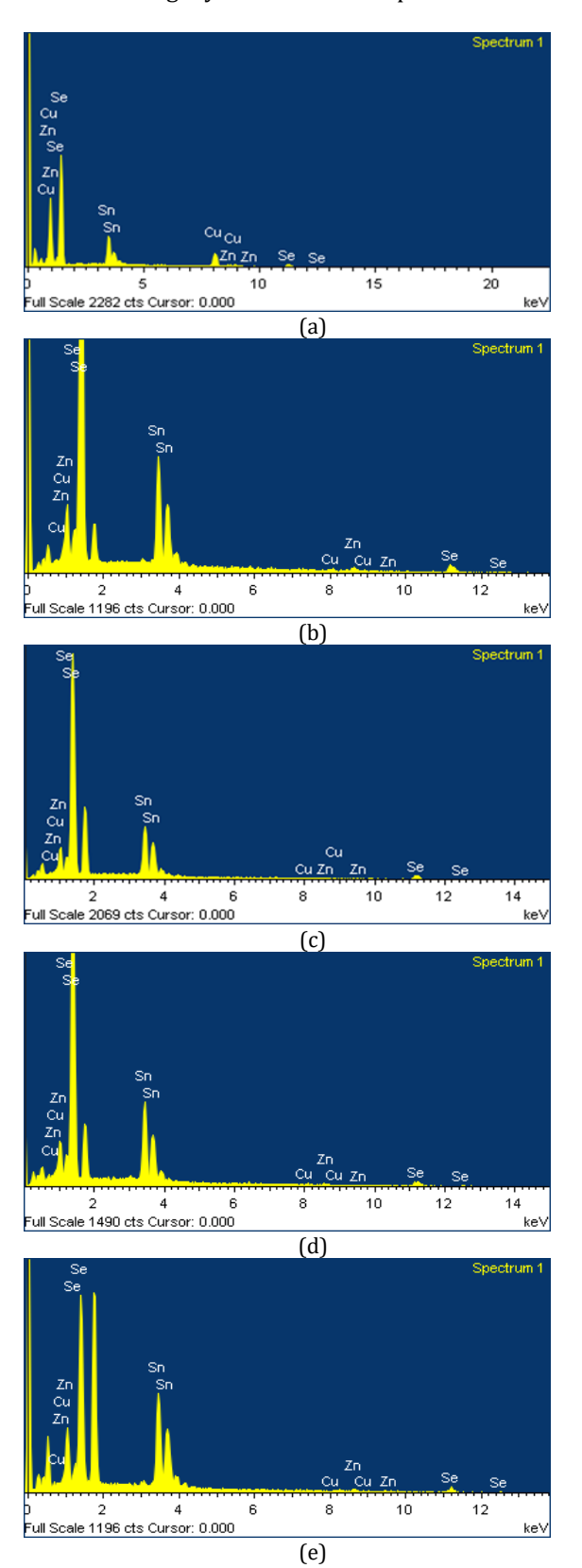


Figure 2. EDAX spectra of (a) CZTSe source material, (b) T0, (c) T400, (d) T500, (e) T600 films

The XRD pattern of the source material is presented in Figure 3. From the diffraction pattern of the source material, considering the intensity and sharpness of

the peaks, one can conclude that the film structure indicates good crystallinity. The obvious peaks could be attributed to (101), (112), (220), (312), (400)\(008), and (316)\(332) planes of Cu₂ZnSnSe₄. The resulting XRD diffraction peaks and planes are well-matched with the International Diffraction Data (ICDD #00-052-0868). Comparable findings have been reported in previous studies [32,33].

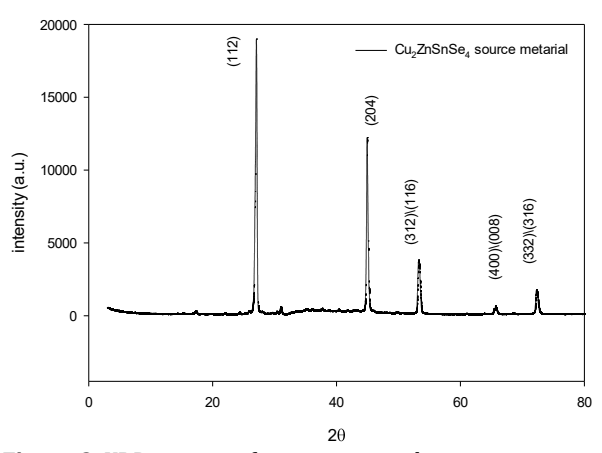


Figure 3. XRD pattern of source material

The X-ray diffractograms of the produced thin films are displayed in Figure 4. From the diffractogram, it is observed that the peak positions of the T0, T500, and T600 samples exhibit identical 2θ values, while the intensities of the peaks increase with annealing. A prominent peak at approximately 21.16° is observed for all samples, with its intensity significantly increasing after thermal treatment at 600 °C. The diffraction peak at this position is attributed to the (110) plane, which is characteristic of the Cu₂ZnSnSe₄ compound. Similar results were also reported in previous studies [21,,34,,35]. A prominent diffraction at $2\theta = 14.31^{\circ}$ indexed to the crystallographic plane was observed exclusively in the XRD pattern of the CZTSe thin film annealed at 400 °C. This peak, which appears as the dominant reflection in the T400 sample, was no longer visible in the patterns of films annealed at 500 °C and 600 °C. The selective emergence of this peak at 400 °C suggests a preferential orientation along the (101) plane, likely stabilized under moderate thermal conditions. At higher temperatures, enhanced atomic diffusion and increased thermal energy are presumed to facilitate structural reorganization, leading to a shift in preferred orientations and the eventual suppression of the (101) reflection. Other researchers have reported similar results for Cu₂ZnSnSe₄ compound produced by different methods [10,,24,,36].

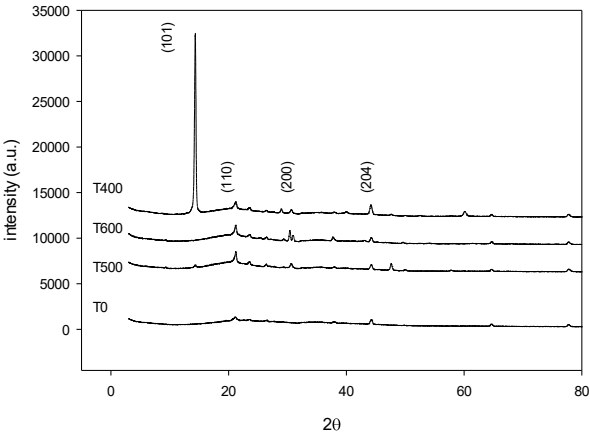


Figure 4. XRD pattern of samples

Raman scattering spectroscopy was employed to investigate the crystallinity of CZTSe, along with the possible formation of secondary phases in the films annealed at various temperatures, as presented in Figure 5. The major peaks obtained from the Raman Spectrum for the CZTSe are expected at between 171-173 cm^{-1} , 194-197 cm^{-1} , and 231-235 cm^{-1} according to the literature [37-39]. In this study, no Raman peaks were observed for the as-deposited samples. All annealed samples exhibited nearly identical Raman spectra, with a prominent peak at approximately 174 cm^{-1} , which is attributed to the kesterite structure of $Cu_2ZnSnSe_4$ thin films [40-42].

The influence of annealing temperature on the evolution of the crystal structure comprehensively examined through XRD and Raman analyses. It was evaluated that the crystal structural changes observed after the annealing process did not affect the chemical composition of the films. In the XRD patterns, the characteristic peaks corresponding to the Cu₂ZnSnSe₄ phase were preserved in all samples, while increases in peak intensities and preferred orientations were observed, attributed to enhanced crystallinity. Therefore, it was concluded that the improvements in the crystal structure did not induce any significant change in the chemical composition.

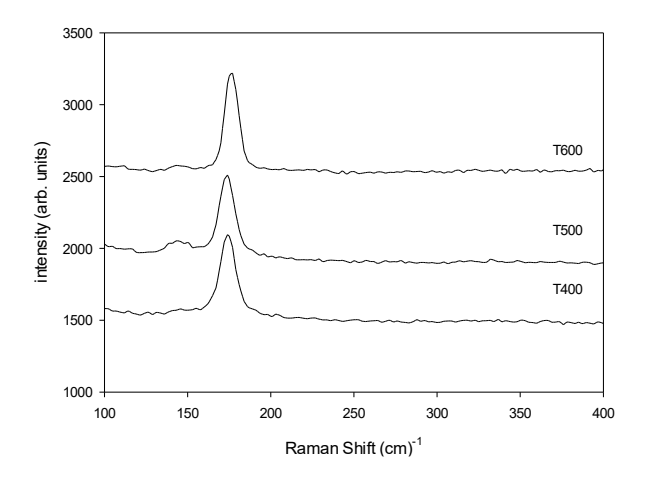


Figure 5. Raman spectra of the annealed films

The electrical conductivity of the samples was obtained through the Van der Pauw technique under vacuum within the temperature interval of 10–400 *K*. The temperature dependent conductivity measurements of the T0 sample could not be measured owing to its high resistivity. The relationship between the logarithm of conductivity and inverse temperature is illustrated in Figure 6. Temperature-dependent measurements revealed that conductivity increases with both measurement temperature and annealing temperature, indicating the semiconducting nature of the films. As shown in Figure 6, the greatest increase in conductivity was recorded for the Cu₂ZnSnSe₄ samples annealed at 500 °C.

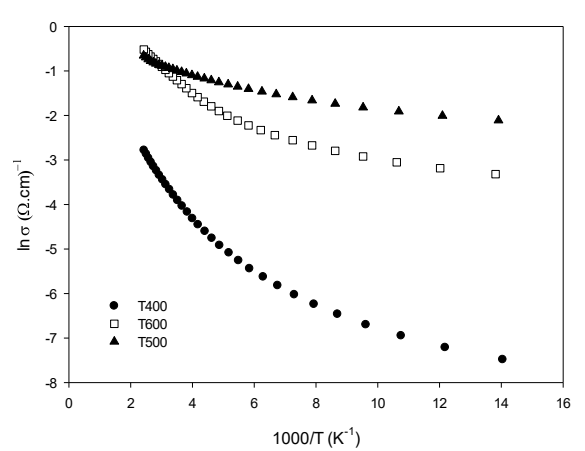


Figure 6. Variation of electrical conductivity with temperature for annealed samples

The room temperature electrical resistivities were measured as around 44.1, 2.61, and 3.08 Ω -cm for the T400, T500, and T600 samples, respectively. The most significant decrease in electrical resistivity was observed in the sample annealed at 500 °C, which can be ascribed to changes in structural parameters and improvements in crystallite and grain size. The enhancement in electrical conductivity observed after annealing is directly associated with improvements in the crystal structure and grain growth. As the annealing temperature increases, the rise in XRD peak intensities indicates an increase in crystallinity and a reduction in structural defects such as vacancies, dislocations, and grain boundaries. The reduction in these defects decreases the number of scattering centers that hinder carrier motion, thereby contributing to increased mobility. Similarly, the grain growth observed in SEM images suggests a decrease in grain boundary density, allowing carriers to move over longer distances with reduced scattering. Consequently, the combined effect of structural ordering and grain enlargement leads to improved electrical conductivity through increased carrier concentration and mobility. This mechanism is consistent with commonly observed scattering behaviors in thin-film semiconductors [43]. Rachmat et al. reported a similar decrease in resistivity. As the substrate temperature increased, the resistivity decreased significantly—from 8.30 to $0.735~\Omega$ -cm [24]. Also, Babu et al. reported a decrease in electrical resistivity from 0.8 to 0.1 Ω -cm with increasing substrate temperature [29]. In a further study, a decrease in resistivity from 58 to 0.16 Ω -cm was reported by Kuo et al. for films fabricated using the DC magnetron sputtering technique [25].

The temperature-dependent electrical conduction was evaluated throughout the whole measurement range using the following relation [44],

$$\sigma = \sigma_0 exp \left(-E_a/kT \right) \tag{1}$$

where σ_0 denotes the pre-exponential factor determined by the material properties, E_a represents the thermal activation energy associated with electrical conduction, and k is the Boltzmann constant. Accordingly, a plot of $\ln \sigma$ versus 1000/T results in a linear relationship with a slope of $-E_a/kT$, from which the activation energy (E_a) can be determined. As presented in Figure 6, the plots of $\ln \sigma$ versus 1000/T exhibit two distinct linear regions, each corresponding to a different activation energy. The depths of the impurity centers, calculated from the electrical conductivity measurements, are provided in Table 2 for annealed samples.

Hall Effect measurements as a function of temperature were conducted to determine the conduction type and to analyze variations in carrier concentration and mobility within the 10--400~K interval. The temperature dependent Hall effect measurements of the T0 sample could not be performed as a result of the high resistivity of the film. Thus, Hall effect measurements were conducted for the T400, T500, and T600 samples. The sign of the Hall voltages revealed that all samples exhibited p-type conductivity.

The dependence of carrier concentration on the inverse temperature within the range of 10-400~K is shown in Figure 7. As illustrated, the carrier concentration increases with temperature, as described by the following expression,

$$p = p_0 exp \left(-E_a/kT \right) \tag{2}$$

The strong temperature dependence and exponential increase of carrier concentration with increasing temperature indicate that thermionic emission, resulting from the thermal excitation of carriers, is the dominant transport mechanism. The increase in carrier concentration, ranging between 10^{15} and 10^{17} cm⁻³ with annealing, can be assigned to improved crystallinity and grain size. Carrier concentrations of Cu₂ZnSnSe₄ films have been reported to range between 10^{17} and 10^{19} cm⁻³, a range which varies with the deposition method [23-26].

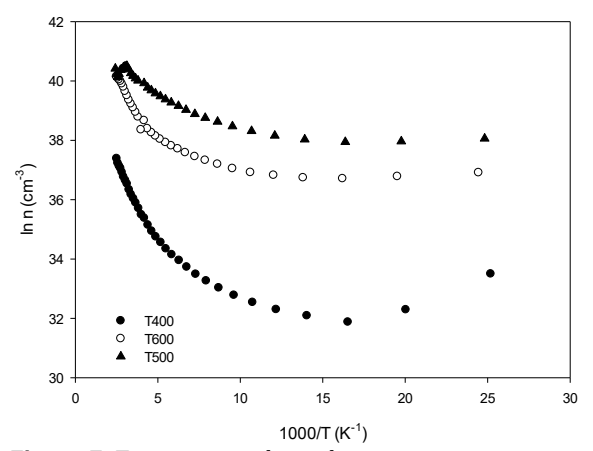


Figure 7. Temperature-dependent carrier concentration of annealed samples

To identify the existing scattering mechanisms, the variation of $Log(\mu)$ with Log(T) was analyzed since the mobility increases with temperature according to the relation $\mu\alpha T^n$, where n defines the dominant scattering mechanism. Room temperature mobilities were found to be 125, 35.3, and 84 $cm^2V^1s^{-1}$ for T400, T500, and T600 samples. Huo Kim et al. reported mobility values in the range of 1.30-9.27 $cm^2V^1s^{-1}$ for thin films, which were fabricated using the simple process of selenization [26].

Table 2. Activation energies and selected electrical parameters of the films evaluated at 295 K

Sample	ρ(Ω-cm)	E _{a1} (meV)	Ea2 (meV)	<i>V_H</i> (<i>V</i>)	μн (cm²V-1s-1)	p (cm) ⁻³
T0	-	-	-	-	-	-
T400	44.1	0.03	48.89	2.92x10 ⁻³	125.0	$5.13x10^{15}$
T500	2.61	9.00	16.98	$0.48x10^{-3}$	35.3	$3.07 x 10^{17}$
T600	3.08	0.94	38.91	1.37x10 ⁻³	84.0	1.07x10 ¹⁷

By changing the selenization temperature and the [Cu]/([Zn]+[Sn]) ratio, mobility values of $Cu_2ZnSnSe_4$ thin films were reported to range from 1.3-80.0 cm^2V

¹S⁻¹. It was reported by Kuo et al. that low Cu content is responsible for low mobilities, while a higher [Zn]+[Sn] ratio results in increased mobility values

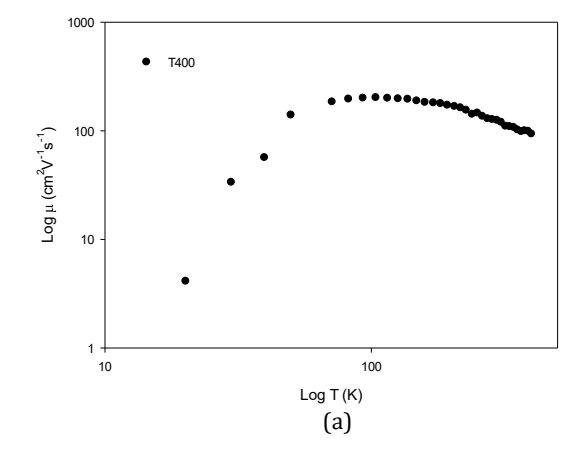
[25]. The mobility of $\text{Cu}_2\text{ZnSnSe}_4$ thin films, reported by other researchers to range from 1.57 to 39.72 $cm^2V^{-1}s^{-1}$ depending on the substrate temperature, was explained by a decrease attributed to scattering and structural imperfections [24]. By varying the Cu/(Zn+Sn) composition ratio in the thin films, mobility values of 1.7, 2.3, and 1.4 $cm^2V^{-1}s^{-1}$ were obtained for Cu/(Zn+Sn) ratios of 1.22, 1.00, and 0.82, respectively [23].

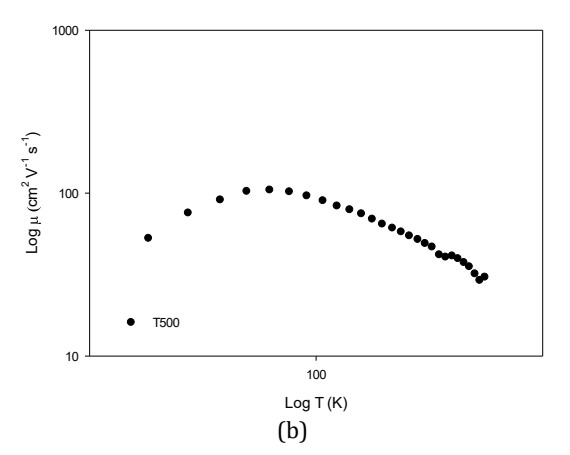
The variation of Hall mobility with temperature for the sample annealed at 400 $^{\circ}C$ is presented in Figure 8(a). At low temperatures (between 20–80 K), the mobility increases with temperature, and the linear variation fits the relation $\mu \alpha T^{3.09}$, which is attributed to ionized impurity scattering as the primary scattering mechanism. In the temperature region above 90 K, a decrease in mobility with increasing temperature is observed, consistent with $\mu \alpha T^{-1/2}$, indicating that polar optical phonon (piezoelectric) scattering is the dominant transport mechanism in this regime [45]. The variation of Hall mobility with temperature for the T500 film is presented in Figure 8(b). In the lowtemperature region (20-50 K), the Hall mobility is dominated by ionized impurity scattering with an exponent of n=1.07. At higher temperatures for the same sample, the mobility decreases with increasing temperature, with n=-0.88, suggesting that hole scattering is mainly attributed to acoustic phonon scattering. The Hall mobility as a function of temperature for the T600 film is shown in Figure 8(c). In the low-temperature range (30–120 K), the Hall mobility is dominated by neutral impurity scattering with n=0.67, arising from unionized donors and neutral defects. At temperatures above 220 K, a decrease in mobility with n=-1.42 indicates that acoustic phonon scattering is the predominant conduction mechanism.

Room-temperature optical absorption measurements were carried out for the thin films in the wavelength range of 190-1100 nm. Generally, the dependence of the absorption coefficient (α) on the incident photon energy (hv) is described by the following equation [46],

$$hv = A(hv - E_g)^n (3)$$

where A denotes a coefficient associated with the transition probability, E_g represents the semiconductor band gap, and n is assigned values of 1/2 for direct transitions and 2 for indirect allowed transitions.





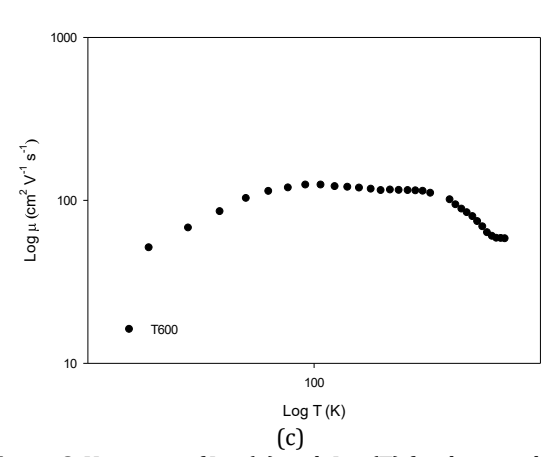


Figure 8. Variation of Log(μ) with Log(T) for the samples (a) T400, (b) T500 and (c) T600

The linear behavior of the plot confirms the presence of a direct transition [47]. Accordingly, the optical band gap values were determined through linear extension of the $(\alpha h \nu)^2$ versus $(h \nu)$ plot toward the energy axis [48]. In Figure 9, the optical absorption spectra of the T0, T400, T500, and T600 thin films are presented in the form of $(\alpha h \nu)^2$ versus $(h \nu)$ plots, from which the band gaps were obtained to be 1.98, 1.78, 1.35, and 1.65 eV, respectively. As illustrated in Figure 9, annealing leads to a decrease in the band gap values of CZTSe thin films, with the lowest value obtained at 500 °C. This significant reduction in band gap at 500 °C may be due to the increase in free carrier concentration and the enhancement in the grain morphology of the films. Similar behavior has also

been reported for $\text{Cu}_2\text{ZnSnSe}_4$ thin films deposited on hot substrates [29]. Depending on the deposition methods and conditions, band gaps were reported to be around ~1.0 eV [28.,31.,49] and ~1.4–1.5 eV [23.,24.,36.,50] for $\text{Cu}_2\text{ZnSnSe}_4$ thin films. Our results are consistent with those obtained in previous studies on co-evaporated [29] and pulsed laser deposited [24] $\text{Cu}_2\text{ZnSnSe}_4$ films.

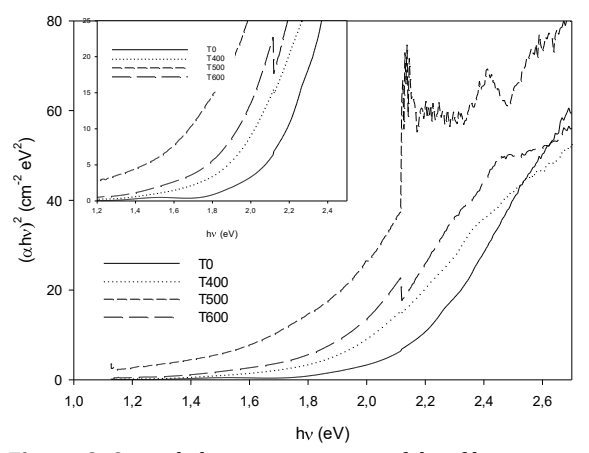


Figure 9. Optical absorption spectra of thin films

4. Conclusions

XRD, SEM, and Raman measurements confirmed that Cu₂ZnSnSe₄ thin films were successfully deposited through thermal evaporation. The experimental results demonstrated that the structural, electrical, and optical properties of the samples are strongly influenced by the annealing treatment. Because of the extremely high resistivity of the as-grown film, measurements could not be performed; however, a considerable decrease in resistivity was observed with annealing, reaching 2.61 Ω -cm at 500 °C. The ptype conductivity of the annealed films was confirmed through Hall effect measurements, with Hall mobility values ranging from 84-125 cm²V⁻¹s⁻¹. The carrier concentration was found to increase from 5.13x10¹⁵ to 3.07×10^{17} cm⁻³, depending on the heat treatment. Absorption studies revealed that the band gaps are direct in nature and were determined to be 1.98, 1.78, 1.35, and 1.65 eV for the as-grown and annealed samples, respectively, with an absorption coefficient of approximately $10^5 \, cm^{-1}$. These band gap values. which can be tuned by heat treatment, are aligned with the optimum band gap required to achieve maximum theoretical conversion efficiency. These results suggest that polycrystalline Cu₂ZnSnSe₄ films produced by the thermal evaporation method could be a promising alternative for the absorber layer in solar cell applications.

Acknowledgment

This study was financially supported by Pamukkale University - Scientific Research Project Center (PAU-BAP) with the project number 2013FBE021.

Declaration of Ethical Code

In this study, we undertake that all the rules required to be followed within the scope of the "Higher Education Institutions Scientific Research and Publication Ethics Directive" are complied with, and that none of the actions stated under the heading "Actions Against Scientific Research and Publication Ethics" are not carried out.

References

- [1] Mufti N., Amrillah T., Taufiq A., Sunaryono, Aripriharta, Diantoro M., Zulhadjri, N., H. 2020. Review of CIGS-based solar cells manufacturing by structural engineering. Solar Energy, 207, 1146-1157.
- [2] Rahman M. F, Chowdhury M., Marasamy L., Mohammed M. K. A., Haque M. D., Al Ahmed S. R., Irfan A., Chaudhry A. R., Goumri-Said S. 2024. Improving the efficiency of a CIGS solar cell to above 31% with Sb₂S₃ as a new BSF: a numerical simulation approach by SCAPS-1D. RSC Advance, 14(3), 1924-1938.
- [3] Reinhard P., Chirila A., Blosch P., Pianezzi F., Nishiwaki S., Buecheler S., Tiwari A. N. 2013. Review of Progress Toward 20% Efficiency Flexible CIGS Solar Cells and Manufacturing Issues of Solar Modules. IEEE Journal of Photovoltaics, 3(1), 572-580.
- [4] Nakamura M., Yamaguchi K., Kimoto Y., Yasaki Y., Kato T., Sugimoto H. 2019. Cd-Free Cu(In,Ga)(Se,S)₂ Thin-Film Solar Cell With Record Efficiency of 23.35%. IEEE Journal of Photovoltaics, 9(6), 1863-1867.
- [5] Jackson P., Hariskos D., Lotter E., Paetel S., Wuerz R., Menner R., Wischmann W., Powalla M. 2011. New world record efficiency for Cu(In,Ga)Se2 thin-film solar cells beyond 20%. Progress in Photovoltaics: Research and Applications, 19(7), 894-897.
 - [6] Bendapudi S. S. K. 2011. Novel Film Formation Pathways for Cu2ZnSnSe4 for Solar Cell Applications. University of South Florida, Master of Science in Electrical Engineering, 18s, Tampa, USA.
- [7] Siebentritt S., Schorr S. 2012. Kesterites—a challenging material for solar cells. Progress in Photovoltaics: Research and Applications, 20(5), 512-519.
- [8] Friedlmeier T., Dittrich H., Schock H. 1998. Growth and Characterization of Cu₂ZnSnS₄ and Cu₂ZnSnSe₄ Thin Films for Photovoltaic Applications. The 11th Conference on Ternary and Multinary Compounds (ICTMC-11), 8-12 September, Salford, UK, 345-348.

- [9] Salomé P. M. P., Fernandes P. A., da Cunha A. F., Leitão J. P., Malaquias J., Weber A., González J.C., da Silva M. I. N. 2010. Growth pressure dependence of Cu₂ZnSnSe₄ properties. Solar Energy Materials and Solar Cells, 94(12), 2176-2180.
- [10] Oh M., Kim W. K. 2014. Sn compensation via SnSe binary vapor supply during Cu₂ZnSnSe₄ formation. Journal of Alloys and Compounds, 616, 436-441.
- [11] Uday Bhaskar P., Suresh Babu G., Kishore Kumar Y. B., Sundara Raja V. 2013. Growth and characterization of Cu₂ZnSnSe₄ thin films by a two-stage process. Solar Energy Materials and Solar Cells, 115, 181-188.
- [12] Shin B., Gunawan O., Zhu Y., Bojarczuk N. A., Chey S. J., Guha S. 2013. Thin film solar cell with 8.4% power conversion efficiency using an earthabundant Cu₂ZnSnS₄ absorber. Progress in Photovoltaics: Research and Applications, 21(1), 72-76.
- [13] Repins I., Beall C., Vora N., DeHart C., Kuciauskas D., Dippo P., To B., Mann J., Hsu W-C, Goodrich A. 2012. Co-evaporated Cu₂ZnSnSe₄ films and devices. Solar Energy Materials and Solar Cells, 101, 154-159.
- [14] Barkhouse D. A. R., Gunawan O., Gokmen T., Todorov T. K., Mitzi D. B. 2012. Device characteristics of a 10.1% hydrazine-processed Cu₂ZnSn(Se,S)₄ solar cell. Progress in Photovoltaics: Research and Applications, 20(1), 6-11.
- [15] Todorov T. K., Tang J., Bag S., Gunawan O., Gokmen T., Zhu Y., Mitzi D. B. 2013. Beyond 11% efficiency: characteristics of state-of-the-art Cu₂ZnSn(S,Se)₄ solar cells. Advanced Energy Materials, 3(1), 34-38.
- [16] Kim S., Kim J. 2013. Effect of selenization on sprayed $Cu_2ZnSnSe_4$ thin film solar cell. Thin Solid Films, 547, 178-180.
- [17] Wang W., Winkler M. T., Gunawan O., Gokmen T., Todorov T. K., Zhu Y., Mitzi D.B. 2014. Device characteristics of CZTSSe thin-film solar cells with 12.6% efficiency. Advanced Energy Materials, 4(7), 1301465.
- [18] Zhou J., Xu X., Wu H., Wang J., Lou L., Yin K., Gong Y., Shi J., Luo Y., Li D. 2022. A precisely regulating phase evolution strategy for highly efficient kesterite solar cells. arXiv preprint arXiv:221013714. (Accessed date: 07.04.2025).
- [19] Wang J., Lou L., Yin K., Meng F., Xu X., Jiao M., Zhang B., Shi J., Wu H., Luo Y. 2024. Vacancy enhanced cation ordering enables> 15% efficiency in Kesterite solar cells. arXiv preprint arXiv:240405974. (Accessed date: 07.04.2025).

- [20] Du Y. F., Zhou W. H., Zhou Y. L., Li P. W., Fan J. Q. He J. J, Wu S. X. 2012. Solvothermal synthesis and characterization of quaternary Cu₂ZnSnSe₄ particles. Materials Science in Semiconductor Processing, 15(2), 214-217.
- [21] Adhi Wibowo R., Hwa Jung W., Kim K. H. 2010. Synthesis of Cu₂ZnSnSe₄ compound powders by solid state reaction using elemental powders. Journal of Physics and Chemistry of Solids, 71(12), 1702-1706.
- [22] Meng M., Wan L., Zou P., Miao S., Xu J. 2013. Cu₂ZnSnSe₄ thin films prepared by selenization of one-step electrochemically deposited Cu–Zn–Sn–Se precursors. Applied Surface Science, 273, 613-616.
- [23] Shao L., Zhang J., Zou C., Xie W. 2012. Cu₂ZnSnSe₄ Thin Films by Selenization of Simultaneously Evaporated Sn-Zn-Cu Metallic Lays for Photovoltaic Applications. Physics Procedia, 32, 640-644.
- [24] Adhi Wibowo R., Soo Lee E., Munir B., Ho Kim K. 2007. Pulsed laser deposition of quaternary Cu₂ZnSnSe₄ thin films. Physica Status Solidi (a), 204(10), 3373-3379.
- [25] Kuo D. H., Hsu J. T., Saragih A. D. 2014. Effects of the metallic target compositions on the absorber properties and the performance of Cu₂ZnSnSe₄ solar cell devices fabricated on TiN-coated Mo/glass substrates. Materials Science and Engineering: B, 186, 94-100.
- [26] Kim K. H., Amal I. 2011. Growth of Cu₂ZnSnSe₄ thin films by selenization of sputtered single-layered Cu-Zn-Sn metallic precursors from a Cu-Zn-Sn alloy target. Electronic Materials Letters, 7(3), 225-230.
- [27] Iljina J., Volobujeva O., Raadik T., Revathi N., Raudoja J., Loorits M., Traksmaa R., Mellikov E. 2013. Selenisation of sequentially electrodeposited Cu–Zn and Sn precursor layers. Thin Solid Films, 535, 14-17.
 - [28] Hong S., Kim C., Park S. C, Rhee I., Kim D. H., Kang J. K. 2012. Characteristics of Cu₂ZnSnSe₄ Film Formed by Using Co-sputtered Precursors and Selenization. Molecular Crystals and Liquid Crystals, 565(1), 147-152.
- [29] Suresh Babu G., Kishore Kumar Y. B., Uday Bhaskar P., Sundara Raja V. 2008. Growth and characterization of co-evaporated Cu₂ZnSnSe₄ thin films for photovoltaic applications. Journal of Physics D: Applied Physics, 41(20), 205305.
- [30] Jung S., Gwak J., Yun J. H., Ahn S., Nam D., Cheong H., Ahn S., Cho A., Shin K., Yoon K. 2013. Cu₂ZnSnSe₄ thin film solar cells based on a single-step co-evaporation process. Thin Solid Films, 535, 52-56.

- [31] Amal M., Kim K. 2012. Optical properties of selenized Cu₂ZnSnSe₄ films from a Cu-Zn-Sn metallic precursor. Chalcogenide Letters, 9(8), 345-353.
- [32] Altosaar M., Raudoja J., Timmo K., Danilson M., Grossberg M., Krunks M., Varema T., Mellikov E. 2006. Cu₂ZnSnSe₄ monograin powders for solar cell application. IEEE 4th World Conference on Photovoltaic Energy Conference, 7-12 May Waikoloa, HI, USA, 468-470.
- [33] Nagaoka A., Yoshino K., Taniguchi H., Taniyama T., Miyake H. 2012. Growth of Cu₂ZnSnSe₄ single crystals from Sn solutions. Journal of Crystal Growth, 354(1), 147-151.
- [34] Lee P. Y., Shei S. C., Hsu E. H., Chang S. J., Chang S. P. 2013. Synthesis of Cu₂ZnSnSe₄ nanocrystals from metal sources using a facile process in isophorondiamine. Materials Letters, 98, 71-73.
- [35] Chou C. S., Su F. C., Chen K., Wu P., Tseng C. S. 2014. Thermo-chemistry guided synthesis of Cu₂ZnSnSe₄ compounds using solvo-thermal method. Advanced Powder Technology, 25(4), 1285-1291.
- [36] Wibowo R. A., Kim W. S., Lee E. S., Munir B., Kim K. H. 2007. Single step preparation of quaternary thin films by RF magnetron sputtering from binary chalcogenide targets. Journal of Physics and Chemistry of Solids, 68(10), 1908-1913.
- [37] Djemour R., Redinger A., Mousel M., Gutay L., Fontane X., Izquierdo-Roca V., Perez-Rodriguez A., Siebentritt S. 2013. The three A symmetry Raman modes of kesterite in Cu₂ZnSnSe₄. Optics Express, 21(Suppl 4), A695-703.
- [38] Dimitrievska M., Oliva F., Guc M., Giraldo S., Saucedo E., Pérez-Rodríguez A., Izquierdo-Roca V. 2019. Defect characterisation in Cu₂ZnSnSe₄ kesterites via resonance Raman spectroscopy and the impact on optoelectronic solar cell properties. Journal of Materials Chemistry A, 7(21), 13293-13304.
- [39] Rakitin V. V., Novikov G. F. 2017. Third-generation solar cells based on quaternary copper compounds with the kesterite-type structure. Russian Chemical Reviews, 86(2), 99-112.
- [40] Mesa F., Leguizamon A., Dussan A., Gordillo G. 2016. Optoelectrical, structural and morphological characterization of Cu₂ZnSnSe₄ compound used in photovoltaic applications. Applied Surface Science, 384, 386-392.
- [41] Kuo S. Y., Lai F. I., Lin K. J., Yang J. F. 2024. Influence of the reaction pathway on the defect concentration of Cu₂ZnSnSe₄ thin film solar cells by manipulation selenization temperature ramping. Sustainable Materials and Technologies, 40, e00920.

- [42] Zaki M. Y., Sava F., Simandan I. D., Stavarache I., Velea A., Pintilie L. 2025. Optimization of CZTSe Thin Films Using Sequential Annealing in Selenium and Tin-Selenium Environments. Inorganic Chemistry, 64(1), 1-10.
- [43] Minnam Reddy V. R., Pallavolu M. R., Guddeti P. R., Gedi S., Bathal Reddy K. K. Y., Pejjai B., Kim W. K., Kotte T. R., Park C. 2019. Review on Cu₂SnS₃, Cu₃SnS₄, and Cu₄SnS₄ thin films and their photovoltaic performance. Journal of Industrial and Engineering Chemistry, 76, 39-74.
- [44] Liu W. J., Xiong G. X., Wang W. P. 2007. Research on synthesis and conductivity of ferrocenyl Schiff base and its salt. Applied Organometallic Chemistry, 21(2), 83-88.
- [45] As D. 1998. Defect related optical and electrical properties of mbe grown cubic GaN epilayers. Radiation effects and defects in solids, 146(1-4), 145-160.
- [46] Pankove J.I. 1975. Optical processes in semiconductors, Dover Publications, New York, USA 34-36s.
- [47] Cabuk M., Yavuz M., Ibrahim Unal H., Alan Y. 2014. Synthesis, characterization, and enhanced antibacterial activity of chitosan-based biodegradable conducting graft copolymers. Polymer Composites, 36(3), 497-509.
- [48] Larbi T., Amara M. A., Ouni B., Amlouk M. 2017. Enhanced photocatalytic degradation of methylene blue dye under UV-sunlight irradiation by cesium doped chromium oxide thin films. Materials Research Bulletin, 95, 152-162.
- [49] Park D., Nam D., Jung S., An S., Gwak J., Yoon K., Yun J. H., Cheong H. 2011. Optical characterization of Cu₂ZnSnSe₄ grown by thermal co-evaporation. Thin Solid Films, 519(21), 7386-7389.
- [50] Chen L. J., Chuang Y. J. 2013. Diethylenetriamine assisted synthesis and characterization of stannite quaternary semiconductor Cu₂ZnSnSe₄ nanorods by self-assembly. Journal of Crystal Growth, 376, 11-16.